Journal of Nuclear Materials 415 (2011) S112–S116

Contents lists available at ScienceDirect

Journal of Nuclear Materials

journal homepage: www.elsevier.com/locate/jnucmat

Analysis of C-MOD molybdenum divertor erosion and code/data comparison ☆

J.N. Brooks [a,*], J.P. Allain [a], D.G. Whyte [b], R. Ochoukov [b], B. Lipschultz [b]

[a] Purdue University, West Lafayette, IN, USA
[b] Massachusetts Institute of Technology, Cambridge, MA, USA

ARTICLE INFO

Article history:
Available online 9 September 2010

ABSTRACT

We analyze an important 15 year old Alcator C-MOD study of campaign-integrated molybdenum divertor erosion in which the measured net erosion was significantly higher (~X3) than originally predicted by a simple model [1,2]. We perform full process sputtering erosion/redeposition computational analysis including the effect of a possible RF induced sheath. The simulations show that most sputtered Mo atoms are ionized close to the surface and strongly redeposited, via Lorentz force motion and collisional friction with the high density incoming plasma. The predicted gross erosion profile is a reasonable match to MoI influx data, however, the critically important net erosion comparison with post-exposure Mo tile analysis is poor, with ~X10 higher peak erosion measured than computed. An RF sheath increases predicted erosion by ~45%, thus being significant but not fundamental. We plan future analysis.

1. Introduction

It is important to understand high-*Z* refractory metal plasma surface performance, for both present devices using molybdenum or tungsten (C-MOD, JET, ASDEX-U), and future devices, notably the ITER W-surface vertical divertor. Recent erosion/redeposition analysis for ITER predicts good (long life) tungsten divertor sputter erosion performance [3], but ongoing validation is needed, e.g., beyond DIII-D tests [4].

The C-Mod campaign was analyzed at the time by a simple "prompt redeposition" model [1,2]. That model did not include most sputtered impurity transport processes. We now analyze the experiment in detail using multi-process coupled codes and with a reassessment of the edge plasma and erosion data.

The coupled code approach of recent studies is used, e.g., [3], with full kinetic/3-D impurity transport modeling, input of divertor geometry, magnetic field, and plasma data, and using binary collision code results for Mo sputter yields and velocity distributions. A kinetic sheath code is used to confirm the oblique-incidence sheath structure for C-MOD, and an ad hoc model is used to study possible RF sheath effects.

2. C-MOD campaign with Mo outer vertical divertor tiles

The 1994–1995 C-MOD campaign used Cr depth-marked Mo divertor tiles exposed to about 1300 s of plasma discharges, with RF powers in the range of 1–2 MW and magnetic fields of ~6–8 T [1,2]. The discharges can be approximately categorized into 1090 shots with eight different divertor plasma conditions, based on shots with one of four plasma currents (600, 800, 1000, 1100 kA), with each shot having an OH and RF heating phase. The RF phases comprised about 30% of the total exposure time. Electron temperatures and densities at and along the vertical divertor ranged from $Te \approx 1$–35 eV, $Ne \approx 0.1$–1×10^{21} m^{-3}, with peak heat fluxes of order 10 MW/m^2, and with shot-dependent strike point locations. For example, for the dominant (55% of total exposure) 800 kA shot the effective (~steady-state) shot length was 1.20 s, with 0.93 s OH and 0.27 s RF phases, and with peak conditions $Te = 20$ eV, $Ne = 1.0 \times 10^{21}$ m^{-3} for the RF phase, and 16 eV, 0.7×10^{20} m^{-3} for the OH phase.

In-shot Mo neutral spectroscopy at the divertor provided an indication of instantaneous gross erosion. Post-campaign ex-situ ion beam (RBS) analysis of removed tiles provided a net erosion profile, showing peak erosion of ~150 nm Mo on the outer vertical target, and with a small region of net deposition [1]. Divertor tile erosion appeared to be due to sputtering only, e.g., no arc tracks or melting was observed [1,5] and no disruptions were reported in the campaign.

3. Modeling

3.1. Impurity transport and plasma parameters

Sputtered molybdenum transport modeling is done using REDEP/WBC code package [6,7] analysis for the (near) vertical, strike-point-containing region of the C-Mod Mo outer divertor;

☆ Work supported by the US Department of Energy, Office of Fusion Energy.
* Corresponding author. Address: Purdue University, 400 Central Drive, West Lafayette, IN 47907-2017, USA. Tel.: +1 765 496 3630; fax: +1 765 494 9750.
E-mail address: brooksjn@purdue.edu (J.N. Brooks).

0022-3115/$ - see front matter © 2010 Elsevier B.V. All rights reserved.
doi:10.1016/j.jnucmat.2010.08.061

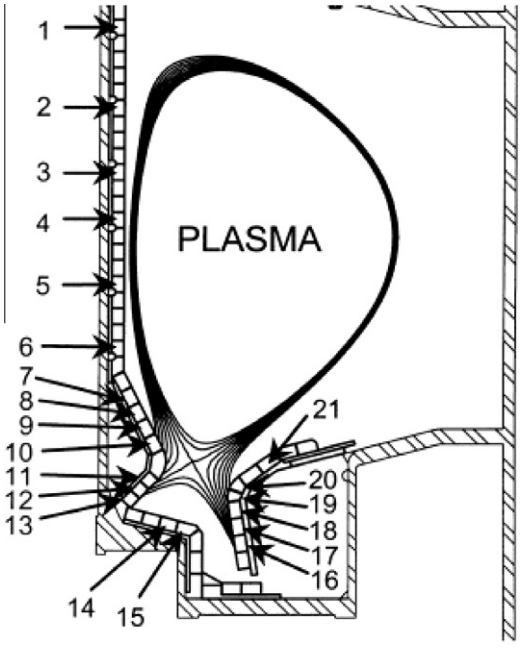

Fig. 1. Alcator C-MOD typical poloidal field lines showing location of Mo divertor tiles with Cr depth marker. From Ref. [1]. Outer vertical divertor, tiles 16–20, analyzed here.

tiles 16–20 of Fig. 1. The WBC Monte Carlo code computes 3-D fully kinetic, sub-gyrorbit transport of surface emitted impurities, with charge-changing and velocity-changing collisions of impurity atoms/ions with the plasma. Sputtering here is due to D^+ plasma ions (charge exchange D^0 sputtering appearing insignificant), with data-inferred 1% Bo^{3+} impingement, and self-sputtering.

Sputtered Mo atoms are launched in WBC per yield and velocity distributions from TRIM-SP code results, for each incident particle species. Electron impact ionization is computed using ADAS rate coefficients (for MoI – MoVI) [8]. A particle history terminates upon redeposition or loss to the plasma (negligible here). Self-sputtering is computed self-consistently per Mo ion redeposition location and energy. (The original modeling [1,2] used a fixed sputtered energy, and treated "prompt redeposition" only, i.e. where ionization/transport occurs within one gyroradius from the surface.)

Plasma parameters per shot, per phase, per tile segment are supplied from C-Mod probe measurements at the divertor plates of density, temperature ($T_i = Te$ assumed) and the local magnetic field. Plasma density at the divertor tiles is modeled as ½ of the probe-defined density and increasing by a factor of two in 1 cm, based on D ionization data. The D and B divertor ion flux is computed from the 3-D magnetic topology, poloidaly varying plasma ion density and temperature data, and assumption of sound speed flow at the divertor. Spectroscopic measurements of the MoI line [2,9] at poloidal locations on the divertor similar to the probe locations were utilized to provide the Mo influx using the S/XB for the emission line. The data for both probes and spectroscopy were interpolated over the region between measurements.

We reviewed the issue of toroidal asymmetry. The C-MOD divertor tiles were curved to conform to toroidal magnetic field lines, and both leading edge and field ripple effects on impurity transport appear small. Toroidal asymmetry effects on erosion/redeposition, as well as diagnostics (e.g., probe toroidal locations different from removed-tile locations) therefore appear to be ignorable for this analysis.

3.2. Sheath model

The BPHI-3D sheath code [10] was run to verify the standard WBC sheath model [6,7] for the near-tangential (~0.6°) C-MOD divertor geometry with representative plasma parameters. Thus, the dual-structure (magnetic + Debye) sheath model is used, with total sheath potential $e\phi = 3kTe$ (25% occurring in the Debye region), locally varying along the divertor, and with Boltzmann factor in-sheath electron density variation. Sheath widths are of order 0.3 mm (magnetic) and 5 μm (Debye).

There is some evidence that ICRF heating can affect C-MOD boundary sheaths—at least for magnetic field lines directly connecting an antenna to a plasma facing surface—by enhancing the transport of electrons to the surface by the "sheath rectification" effect [9,11]. However, for the tiles in question (as opposed to the top of the divertor) the field lines are not directly connected to the antenna, thus possibly increasing the sheath potential but not as much as for the direct-connection case. No rigorous model exists for this case [12]. To roughly assess this we use an ad hoc RF sheath REDEP model assuming doubling of the locally varying sheath potential, i.e. $e\phi = 6kTe$. RF heating is assumed to affect the sheath potential only; no effect on sheath width or structure, if any, is modeled (or would appear to be highly significant).

3.3. Sputter yields/velocity distributions

The TRIM-SP binary collision code is used to compute sputter yields for a pure Mo surface. This is a version of the TRIM code [13]. TRIM-SP uses an equipartition between the local Oen-Robinson inelastic energy loss model and the non-local Lindhard–Sharff inelastic energy loss model. The simulations for molybdenum use a surface binding energy of 6.83 eV, based on the heat of sublimation. A pure Mo surface is justified based on dynamic Monte Carlo ion-mixing simulations using the newly developed DYNIMIX code. Results show that for energies in the range between 10–1000 eV B on Mo, the near-surface concentration of B is ⩽15% (atomic fraction) in a region about 2 nm deep. This is consistent with ex-situ post-mortem surface analysis of the Mo tiles by Wampler et al. [1]. This small amount of B only affects the Mo sputter yield by about 5%.

Fig. 2 shows TRIM-SP sputter yields for D, B, Mo, for characteristic C-MOD divertor WBC-computed impingement angles (from normal). Sputtered energy distributions generally match the

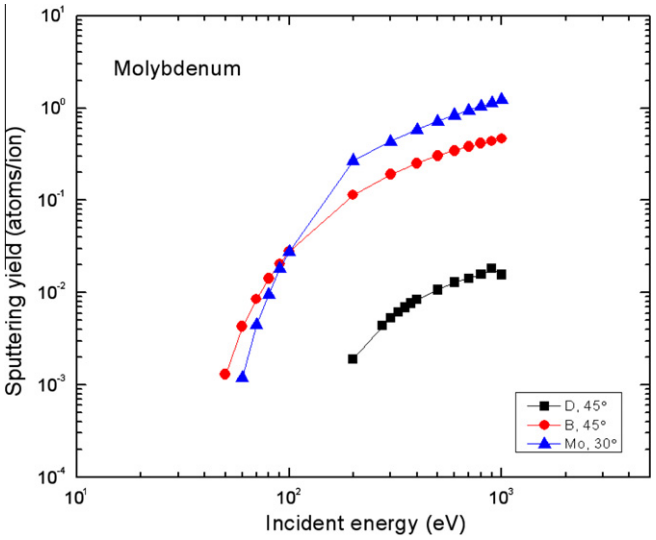

Fig. 2. TRIM-SP results for D, B, Mo sputtering of Mo.

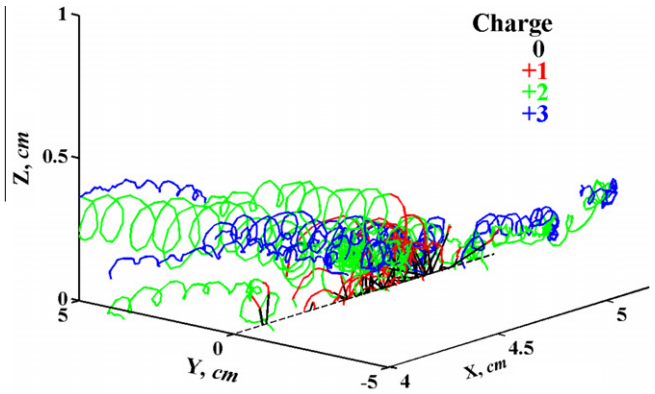

Fig. 3. WBC code computed 50 typical sputtered Mo histories; for particles launched near middle of C-MOD outer vertical divertor, for 800 kA shot OH phase. Coordinates: "X" along divertor from top-to-bottom (X = 4.5 cm is 50.5 cm poloidaly below midplane, at tile 17), "Y" along toroidal magnetic field, "Z" perpendicular to divertor (note scale differences). (Trajectories computed for full divertor zone; $0 \leqslant X \leqslant 11$ cm, $-1.9 \leqslant Y \leqslant 1.9$ m, $0 \leqslant Z \leqslant 5$ cm; but shown here for partial region only).

Table 1
WBC C-MOD transport summary for sputtered molybdenum, for the 800 kA shot (over entire divertor region analyzed).

Parameter	OH phase	RF phase (no RF sheath)	RF phase w/RF sheath
Ionization mean-free-path[a]	0.466 mm	0.754 mm	0.872 mm
Transit time[b]	2.33 μs	4.76 μs	4.96 μs
Charge state[c]	1.82	1.94	1.95
Energy[c]	129 eV	162 eV	278 eV
Incidence angle, from normal[c]	30.5°	29.6°	24.2°

[a] For sputtered Mo atoms, perp. to surface.
[b] Average for Mo ions from ionization to redeposition.
[c] Average for redeposited Mo ions.

Thompson distribution at low sputtered energy ($\leqslant$10 eV) with peaking at half the binding energy, but with sharper falloff than Thompson (as expected from binary collision considerations), and, e.g., for B on Mo, with maximum sputtered energy in the range ~20–100 eV depending on incident energy.

4. Results

Simulations were made for the reference case (no RF sheath), with RF sheath, and for several model variations; each computer run uses ~10^6 sputtered particle histories. Fig. 3 shows typical histories, in this case for the 1 cm near-middle region of the divertor, for the OH phase of the 800 kA shot, and Table 1 summarizes all histories for this shot. The simulations show a basic picture of most sputtered Mo atoms ionized close (<1 mm) to the surface, by electron impact ionization, and strongly redeposited via Lorentz force motion and collisional friction with the incoming plasma. Per Fig. 1, a number of ions travel further, primarily in the toroidal direction, undergoing gyro-rotation, elastic collisions with the background plasma, and ionization into higher charge states. Overall redeposition fraction on the entire divertor zone analyzed is essentially 100%, while local (point) redeposition fractions vary from ~95–105%.

Boron sputtering dominates the reference case erosion, with self-sputtering being about a 15–20% effect, depending on plasma condition, and with D sputtering contributing about 5% of the total campaign erosion. With the RF enhanced sheath, Mo and D sputtering rise to ~35% and ~15% respectively, for erosion during the RF periods.

Fig. 4 shows the code/data *gross erosion rate* comparison for selected shots. Comparisons for the other shots show similar trends. For the 800 kA standard sheath case (4a) the peak simulation values are in reasonable agreement (~factor of 2) with the peak data values, for both the OH and RF phases. The simulations show a broader erosion profile than the data, particularly for the OH phase. Addition of the RF enhanced sheath (4b) increases the predicted RF phase erosion, but with similar profile. The increased erosion is simply due to increased sputter yields for the higher sheath-acquired ion impingement energies. Fig. 4c for the 1000 kA shot shows a generally good code/data match, but with the peak data value better matching the RF sheath case.

Fig. 5 shows the code/data comparison for *campaign-integrated gross erosion*. The measurement points here are computed by convolving the erosion rate (spectroscopic) data with the shot/phase time durations. The reference case code/data match is within about a factor of two, over most of the divertor. The RF sheath case simulation better matches the peak data erosion, but is about 2–3× higher for several other points.

Fig. 6 shows the code/data comparison for *campaign-integrated net erosion*. The *simulation* shows several trends: (1) Peak net erosion is about a factor of 30 less than the corresponding gross erosion, with net erosion depending on a fine balance between erosion and redeposition. (2) Transfer of sputtered Mo from top-to-bottom of the divertor, resulting in net deposition (growth) on the lower portion. Such transfer is clearly explainable, in principle, by the poloidal magnetic field line structure, and is predicted in similar angled-field divertor simulations (e.g., ITER, DIII-D). (3) No net loss of material from the vertical divertor as a whole. (4) Increase in peak net erosion of ~45% due to the RF sheath.

The net erosion *data* shows three key trends: (1) Factor of ~3–10 erosion reduction from gross erosion, thus much less reduction

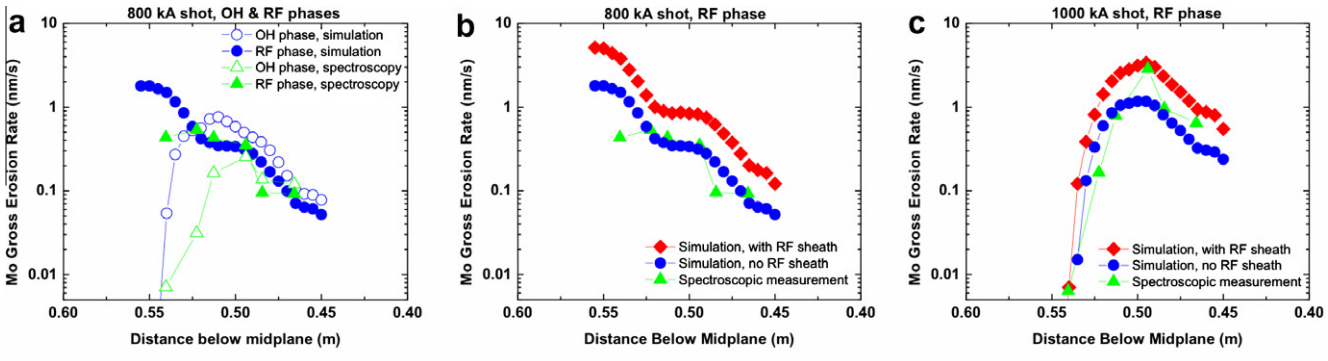

Fig. 4. Code/data comparisons of gross erosion rate: (a) 800 kA shot no RF sheath, (b) 800 kA shot w/ and w/o RF sheath, (c) 1000 kA shot w/ and w/o RF sheath.

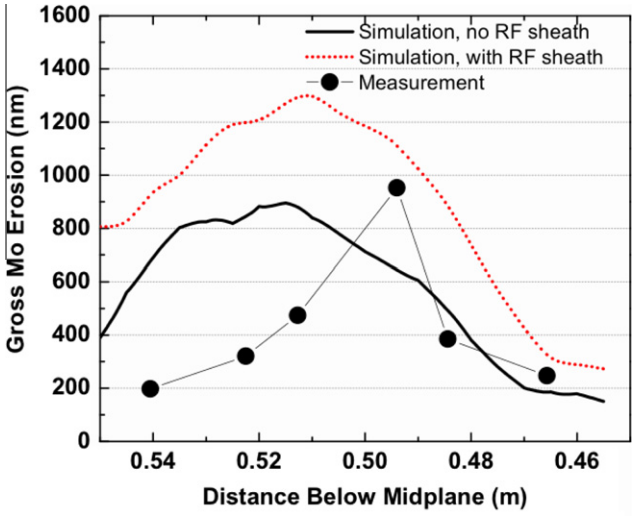

Fig. 5. Predicted vs. measured gross erosion over campaign.

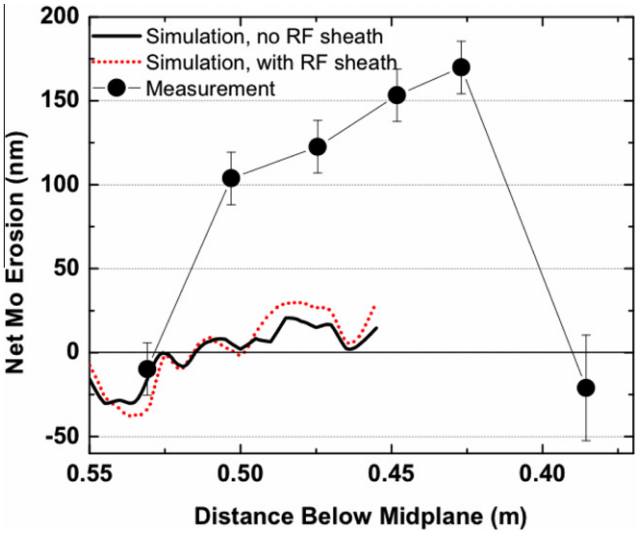

Fig. 6. Predicted vs. measured net erosion over campaign.

than predicted. (2) Top-to-bottom Mo transfer with resulting growth region at the bottom, similar to code prediction. (3) Net loss of material from the vertical divertor, again in contrast to prediction.

In summary, there is a major code/data mismatch for the net erosion. The predicted peak net erosion is ~20–30 nm, depending on the RF sheath factor, vs. ~150 nm data in the region simulated. Considering that the predicted gross erosion would generally better match the data with a somewhat lower boron content, thus proportionally lowering the predicted net erosion, we conclude that there is roughly an order of magnitude discrepancy between the campaign-integrated net erosion prediction, and the post-experiment, marker-tile erosion diagnostic data.

5. Model variations

We studied several variations in impurity transport models. The computed gross erosion is not significantly changed (~±15%) with any variation explored. In terms of net erosion, a factor of 10 reduction from the reference WBC velocity-changing collision rate model (extended Braginskii theory) makes no significant difference, due to the already very high baseline collision rates; this is also true of a factor of 10 reduction in at-divertor plasma Mach number. An extreme factor of 100 reduction in collisions, or completely eliminating collisions, results in ~2–3× higher peak net erosion, due to the loss (non-divertor redeposition) of 5–10% of the sputtered Mo. However, this extreme change in collision model also results in no predicted growth region, thus not matching this aspect of the data. (We also note that such radical change in the plasma model would affect more than Mo transport, namely our entire understanding/prediction of SOL/edge plasma transport.) A change in the particle anomalous diffusion coefficient from the locally-varying Bohm value to a fixed and higher 1 m^2/s value results in a ~25% increase in peak net erosion. Finally, several changes in the magnetic geometry model corresponding to various uncertainties do not make a large difference. In summary of the variation effects, no variation studied resolves the major code/data net erosion difference.

6. Discussion

There are still some model limitations, believed reasonable for the present study. In addition to the ad hoc RF sheath model, the surface-response/sputter-yield simulations do not account for ion-induced phase transformations or morphology evolution that could occur during plasma irradiation over the course of a year's C-MOD campaign. Also, there are various numerical approximations regarding use of the sputter calculations (e.g., angular distribution treated as separable from energy distribution), plasma parameter interpolation, and the like. It appears unlikely that these limitations affect the order-of-magnitude net erosion discrepancy, also considering that there is a reasonable match to the gross erosion.

The net erosion data [1] showed apparent high Mo growth regions (e.g., ~100 nm for inner wall tile 5)—such growth would be difficult to explain via existing plasma transport and erosion/redeposition theory. We are informed [5], however, that error bars for the growth-region diagnostic tiles are higher than initially reported, due to high boron deposition, thus making conclusions difficult. This is not considered a problem for the erosion-dominated, low-B-content, outer strike point (OSP) region modeled here.

A possible explanation for the net erosion discrepancy is that high heat deposition could have led to enhanced erosion of the OSP diagnostic tiles thin-film marker coatings (300–600 nm Mo on 100 nm Cr). It is well known that thin-films can be highly susceptible to thermo-mechanical stresses, in this case possibly leading to partial Mo layer peel-off (generally more likely than full film loss). This depends on film conformality, density, adhesion, and surface-roughness. Obviously, such higher erosion could account for the code/data discrepancy, but evidence (e.g., surface morphology data) is lacking one way or the other.

7. Conclusions

This analysis of the C-MOD Mo erosion campaign with advanced computational modeling shows the typically predicted pattern of high-Z divertor intense redeposition of sputtered material, with order of magnitude reduction in net vs. gross erosion. The instantaneous and campaign-integrated gross erosion predictions are a reasonable match to the spectroscopically derived data, particularly considering the number, duration, and complex nature of the plasma shots. The analysis shows that most Mo sputtering is due to the boron impurity, with low D sputtering and moderate self-sputtering. A hypothetical increase (doubling) of the sheath

potential by RF heating effects increases erosion, but without self-sputtering runaway, for this low temperature high density divertor plasma regime.

The low gross sputtering erosion (e.g., compared to Be or C), by itself, is encouraging for high-Z material use in future devices, e.g., ITER, where anticipated divertor plasma parameters are similar to C-MOD. However, there is a major discrepancy for net erosion, with the post-exposure marker-tile data showing much higher net Mo erosion than predicted. A review of the original plasma probe, magnetic field, and spectroscopic data has identified no obvious defect, and likewise for divertor toroidal symmetry assumptions.

This work shows a need for further code/data erosion/redeposition validation, ideally with short exposure conditions and advanced diagnostics, and we plan to do this for upcoming C-MOD experiments. There remains a major need for supercomputer erosion/redeposition modeling, e.g., with full plasma/sputter/impurity-transport code-coupling, and with rigorous RF sheath and surface evolution modeling.

References

[1] W. Wampler et al., Journal of Nuclear Materials 266–269 (1999) 217.
[2] D.A. Pappas et al., Journal of Nuclear Materials 266–269 (1999) 635.
[3] J.N. Brooks et al., Nuclear Fusion 49 (2009) 035007.
[4] J.N. Brooks, D.G. Whyte, Nuclear Fusion 39 (1999) 525.
[5] W. Wampler, Sandia National Laboratories, Personal Communication, 2010.
[6] J.N. Brooks, Fusion Engineering and Design 60 (2002) 515.
[7] J.N. Brooks, Physics of Fluids 8 (1990) 1858.
[8] The Originating Developer of ADAS is the JET Joint Undertaking.
[9] B. Lipschultz et al., Nuclear Fusion 41 (2001) 585.
[10] J.N. Brooks, D. Naujoks, Physics of Plasmas 7 (2000) 2565.
[11] S.J. Wukitch et al., Journal of Nuclear Materials 363–365 (2007) 491.
[12] D.A. D'Ippolito, Lodestar Co., Personal Communication, 2009.
[13] J.P. Biersack, W. Eckstein, Journal of Applied Physics A34 (1984) 73.